A&A 465, 1099–1108 (2007)
DOI: 10.1051/0004-6361:20065358
© ESO 2007

Astronomy & Astrophysics

New spectroscopic redshifts from the CDFS and a test of the cosmological relevance of the GOODS-South field⋆

C. D. Ravikumar[1,2], M. Puech[1], H. Flores[1], D. Proust[1], F. Hammer[1], M. Lehnert[3,1], A. Rawat[4,1], P. Amram[5], C. Balkowski[1], D. Burgarella[5], P. Cassata[6], C. Cesarsky[7], A. Cimatti[8], F. Combes[9], E. Daddi[10,12], H. Dannerbauer[11], S. di Serego Alighieri[8], D. Elbaz[12], B. Guiderdoni[13,2], A. Kembhavi[4], Y. C. Liang[14], L. Pozzetti[15], D. Vergani[1], J. Vernet[7], H. Wozniak[13], and X. Z. Zheng[11]

[1] GEPI, Observatoire de Paris-Meudon, 92195 Meudon, France
e-mail: Chazhiyat.Ravikumar@obspm.fr
[2] Institut d'Astrophysique du CNRS, 98bis Boulevard Arago, 75014 Paris, France
[3] Max-Planck-Institut für extraterrestrische Physik, Giessenbachstrasse, 85748 Garching bei München, Germany
[4] Inter University Center for Astronomy & Astrophysics, Post Bag 4, Ganeshkhind, Pune 411007, India
[5] Laboratoire d'Astrophysique de Marseille, Observatoire Astronomique de Marseille-Provence, 2 place Le Verrier, 13248 Marseille, France
[6] Dipartimento di Astronomia, Vicolo Osservatorio 2, 35122 Padova, Italy
[7] ESO, Karl-Schwarzschild Strase 2, 85748 Garching bei München, Germany
[8] INAF, Osservatorio Astrofisico di Arcetri, Largo Enrico Fermi 5, 50125 Florence, Italy
[9] LERMA, Observatoire de Paris, 61 Av. de l'Observatoire, 75014 Paris, France
[10] National Optical Astronomy Observatory, 950 North Cherry Avenue, Tucson, AZ 85719, USA
[11] MPIA, Königstuhl 17, 69117 Heidelberg, Germany
[12] CEA Saclay/DSM/DAPNIA/Service d'Astrophysique, Orme des Merisiers, 91191 Gif-sur-Yvette Cedex, France
[13] Centre de Recherche Astronomique de Lyon, 9 avenue Charles Andr, 69561 Saint-Genis-Laval Cedex, France
[14] National Astronomical Observatories, Chinese Academy of Sciences, 20A Datun Road, Chaoyang District, Beijing 100012, PR China
[15] INAF – Osservatorio Astronomico di Bologna, via Ranzani 1, 40127 Bologna, Italy

Received 4 April 2006 / Accepted 28 November 2006

ABSTRACT

Context. This paper prepares a series of papers analysing the Intermediate MAss Galaxy Evolution Sequence (IMAGES) up to a redshift of one. Intermediate mass galaxies ($M_J \leq -20.3$) are selected from the Chandra Deep Field South (CDFS) for which we identify a serious lack of spectroscopically determined redshifts.
Aims. Our primary aim in this study is therefore to obtain a sample of intermediate-mass galaxies with known spectroscopic redshift to be used for further analysis of their 3D-kinematics. We also intend to test whether this important cosmological field may be significantly affected by cosmic variance.
Methods. The spectroscopic observations were carried out using VIMOS on the ESO VLT. The data reduction was done using a set of semi-automatic IRAF procedures developed by our team.
Results. We have spectroscopically identified 691 objects including 580 galaxies, 7 QSOs, and 104 stars. The overall completeness achieved is about 76% for objects with $I_{AB} \leq 23.5$ in the CDFS after excluding instrumental failures. This study provides 531 new redshifts in the CDFS. It confirms the presence of several large-scale structures in the CDFS, which are found to be more prominent than in other redshift surveys. To test the impact of these structures in the GOODS-South field, we constructed a representative redshift catalog of 640 galaxies with $I_{AB} \leq 23.5$ and $z \leq 1$. We then compared the evolution of rest-frame U, B, V, and K galaxy luminosity densities to the one derived from the Canada France Redshift Survey (CFRS). The GOODS South field shows a significant excess of luminosity densities in the $z = 0.5$–0.75 range, which increases with the wavelength, reaching up to 0.5 dex at 2.1 μm. Stellar mass and specific star formation evolutions might be significantly affected by the presence of the peculiar large-scale structures at $z = 0.668$ and at $z = 0.735$, which contain a significant excess of evolved, massive galaxies when compared to other fields.
Conclusions. This leads to a clear warning about the results based on the CDFS/GOODS South fields, especially those related to the evolution of red luminosity densities, i.e. stellar mass density and specific star formation rate. Photometric redshift techniques, when applied to that field, are producing quantities that are apparently less affected by cosmic variance (0.25 dex at 2.1 μm), however, at the cost of any ease in disentangling the evolutionary and cosmic variance effects.

Key words. galaxies: high-redshift – galaxies: distances and redshifts – cosmology: observations – galaxies: evolution – cosmology: large scale structure of Universe – surveys

1. Introduction

Studies suggest growing evidence of a significant evolution in the ensemble of galaxies out to $z = 1$. Analysis of stellar population of galaxies shows that the bulk of star formation occurs between $z = 1$ and $z = 0.4$, mostly dominated by star formation

⋆ Table 2 is only available in electronic form at the CDS via anonymous ftp to cdsarc.u-strasbg.fr(130.79.128.5) or via http://cdsweb.u-strasbg.fr/cgi-bin/qcat?J/A+A/465/1099

Article published by EDP Sciences and available at http://www.aanda.org or http://dx.doi.org/10.1051/0004-6361:20065358

in galaxies in the range 3–30 × 10^{10} $M_\odot$ (Heavens et al. 2004; Hammer et al. 2005). This increased star formation activity is reflected in the strong evolution shown by galaxies in this redshift range from the analysis of the 15 μm observations by ISOCAM (Elbaz et al. 2002). These infrared- selected galaxies with their high star formation rate, averaging ∼100 $M_\odot$/yr, contribute significantly to the star formation history (Flores et al. 1999; Le Floc'h et al. 2005 and the references therein). The luminous infra-red galaxies (LIRGs) are up to 40 times more numerous at $z \sim 1$ than locally, and such a strong luminosity evolution has been attributed to the rapidly increased frequency of interactions ($(1+z)^{3-4}$ for $z \leq 1$; see e.g. Hammer et al. 2005). However, major merging events appear to drive the high star-formation rates of only about 30% of LIRGs (Flores et al. 1999; Zheng et al. 2004). Interestingly, some of these star-forming galaxies appear to be large, massive disk galaxies, thus emphasizing the important role of studying the dynamics of intermediate mass (3–30 × 10^{10} $M_\odot$) galaxies for understanding galaxy evolution.

Through the ESO large program "Intermediate MAss Galaxies Evolution Sequence (IMAGES)" we intend to (1) establish the evolution of mass-to-light ratio; (2) test the different physical processes leading to the present day Hubble sequence; (3) explain the star formation history of each individual galaxy; and (4) test the evolution of mass-metallicity relation, angular momentum, size, and mass. The analysis involves combining GIRAFFE and FORS2[1] observations being carried out of a sample of intermediate mass galaxies, selected mainly by their rest-frame $J_{\rm AB}$ magnitude, derived from the multi-wavelength photometric data available. The 3D spectroscopic observations using GIRAFFE (e.g. Flores et al. 2004) can provide detailed kinematics (e.g. Puech et al. 2006a) including accurate Tully-Fisher relations (Tully & Fisher 1977; see Flores et al. 2006). It can also provide electron density maps of distant galaxies (Puech et al. 2006b), thanks to the high spectral resolution ($R \sim 10\,000$) of the instrument allowing the [OII]$\lambda\lambda$3726,3729 doublet to be easily resolved. Besides this, we derive the chemical abundances of galaxies using observations with FORS2 (Appenzeller et al. 1998), taking advantage of its excellent red sensitivity.

The sample of intermediate-mass galaxies for our study IMAGES is selected mainly by their rest frame J_{AB} magnitudes ($M_{\rm J}(AB) \leq -20.3$) corresponding to stellar masses greater than 1.5 × 10^{10} $M_\odot$. Because the CDFS represents one of the most deeply surveyed at all wavelengths, we have chosen to carry out IMAGES in this field. Unfortunately, in the CDFS, this galaxy population had insufficient numbers of spectroscopic redshifts available. The VVDS (Vimos VLT Deep Survey, Le Fèvre et al. 2004), FORS2 (Vanzella et al. 2005, 2006), and K20 (Mignoli et al. 2005) surveys were intentionally designed to focus on faint magnitudes (typically $I_{AB} \leq 24$) in order to preferentially identify objects at higher redshifts, which results in essentially picking up fainter (and hence low-mass) objects in the redshift range we are interested in ($0.4 \leq z \leq 0.9$). With the redshift survey discussed here, we intend to increase the number of redshifts of relatively bright and emission line galaxies. When studying the evolution of galaxies in a particular field, one must pay careful attention to how representative the field is, for example, in its redshift distribution. The existence of one or several significant peaks in the redshift distribution of the CDFS, indicating the presence of large-scale structures, might be problematic in interpreting the results when studying galaxy evolution, such as the GOODS or IMAGES programs.

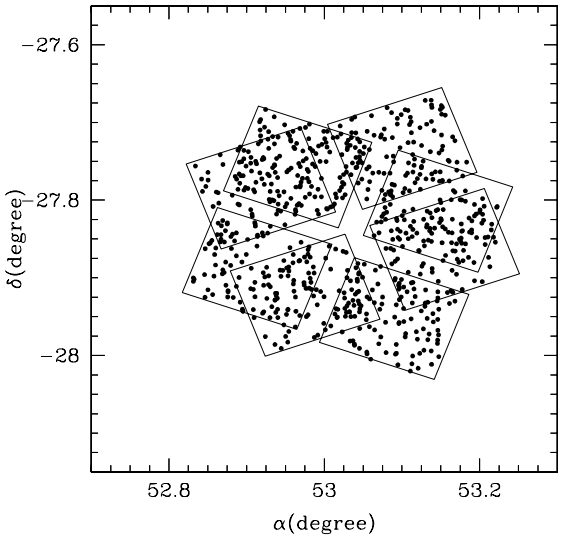

Fig. 1. The two pointings by VIMOS in the CDFS covering roughly the same area in the sky as in the VVDS. The black dots are the positions of the objects for which we have determined redshifts. A sample of 969 objects with $I_{AB} \leq 23.5$ were selected for observation constituting ∼25% of galaxies on the field.

The structure of the paper is as follows. In Sect. 2 we describe the observation and data reduction of low-resolution VIMOS spectra from the CDFS, and in Sect. 3 we provide the general properties of the sample for which we obtain redshifts. Further more, we analyze the cosmological relevance of GOODS in Sect. 4 by constructing a representative spectroscopic catalog paying attention to the selection biases involved. Finally, we provide a conclusion in Sect. 5. We adopt the Λ−CDM cosmological model ($H_0 = 70$ km s^{-1} Mpc^{-1}, $\Omega_{\rm M} = 0.3$, and $\Omega_\Lambda = 0.7$). Also, all magnitudes used in this paper are in the AB system, unless explicitly noted otherwise.

2. Observations

We carried out the spectroscopic observations with VIMOS on the VLT-UT3 Melipal during December 3–4, 2004. The observing conditions were photometric and the seeing was ∼1 arcsec. The low-resolution red grism, LRRED, was used with a slit width of 1 arcsec. The spectral resolution in this mode is 34 Å at 7500 Å or $R \sim 220$. The red bandpass filter, which also serves for order separation, limits the spectral range to 5500–9500 Å. A complete VIMOS pointing consists of observations with four quadrants of the instrument each separated by about 2 arcmin from its neighbor. We have set two pointings around the CDFS as shown in the Fig. 1 with an angle of ∼90 degrees between them. The total area covered is ∼370 arcmin^2 on the sky. An integration time of 45 min was given per pointing. Given the short exposure time, we have concentrated the slits mainly on galaxies of the field with $I_{AB} \leq 23.5$ in order to complement the existing deeper surveys. The positions of the objects for which we could estimate redshifts are also shown in Fig. 1.

The slit masks were prepared using the photometric catalog from the ESO Imaging Survey (Arnouts et al. 2001) and the I-band VIMOS pre-images. The VMMPS code[2] was run to

[1] For a description of the instruments, the GIRAFFE & FORS2, see http://www.eso.org/instruments/

[2] http://134.171.56.104/observing/p2pp/OSS/VMMPS/VMMPS-tool.html

Table 1. Number and type of objects in the classes, secure (2), insecure (1) and single emission line (9), for which we have determined redshifts.

Class	Galaxy	Star	QSO	Total	%
2	308	88	6	402	35.2
1	206	16	1	223	19.5
9	66	–	–	66	5.8
Total				691	60.5

optimize the number and positions of the slits for each quadrant. However, we carried out a final re-arrangement of the slits by hand in order to improve the number of objects observed. This resulted in placing a total of 1142 slits in the two pointings, among which 969 were objects with $I_{AB} \leq 23.5$.

Data reduction and extraction of the optical spectra were performed by three of us (CDR, HF, and DP) using a set of semi-automatic IRAF[3] procedures developed by our team. The routines allowed us to simultaneously reconstruct the spectra of the object and the surrounding sky. The spectra were flux-calibrated using two standard stars. Images in the V, R, and I bands were used to check the slope of our spectra.

2.1. Redshifts

The redshift determination of each spectrum from all the eight quadrants was done independently by three team members (CDR, HF, & DP), making sure that each spectrum was analyzed by at least two members. When the individual estimates of the redshifts among the three members did not agree, measurements were examined by a fourth team member (FH). When the fourth team member agreed with neither of the previous independent estimates, that object was discarded. Each redshift measurement was associated with a "quality" flag denoting the reliability of the extraction. The low signal-to-noise, mainly due to the short total integration time, allowed us to classify the reliability into just four classes; secure (class = 2), insecure (1), single emission-line (9), and failed (0) observations. Secured spectroscopic identifications contain more than two strong features, while sources classified as insecure contain either a strong feature with not very reliable supporting features, or with multiple features that are not strong enough to confirm the redshift, giving a confidence of only about 50% to the estimated redshift. Class (9) sources correspond to spectra with a single strong emission line without any other features. Redshifts are tentatively assigned for such cases. Typically this is the case where we are unable to differentiate [OII]λ3727 and Hα emission lines. The failed class contains spectra for which we could not obtain a redshift, mainly due to low signal-to-noise or to reasons that have an instrumental origin, like the presence of bad pixels or an object near the boundary of the slit.

Figure 2 shows the sample spectra for the different classes used. In addition to this, we have provided each redshift with a type classification to show that the observed spectrum belongs to an emission line galaxy (type = 1), an absorption line galaxy (2), a quasar (3), or a star (4). In Table 1 we show the number and type of objects in the different classes along with the percentage (%) of objects for which redshifts are obtained out of the 1142 slits placed. For about 12% of objects we were not able to determine the redshift because of instrument-related problems.

[3] IRAF is distributed by the National Optical Astronomy Observatories, which are operated by the Association of Universities for Research in Astronomy, Inc., under cooperative agreement with the National Science Foundation.

2.2. The redshift catalog

The catalog lists spectroscopic data for 691 objects from the CDFS, containing 580 galaxies, 104 stars and 7 QSOs (see Tables 1 and 2[4]). In the catalog (Table 2) we provide for each object:

- the ESO imaging survey (EIS) identification number and equatorial coordinates (equinox 2000);
- the class and type codes denoting the quality and nature of the spectra, as described in the previous section;
- the redshift measured by the IMAGES team;
- the internal identifier;
- the isophotal I_{AB} band magnitude from Arnouts et al. (2001) and the derived absolute magnitudes (AB system) following Hammer et al. (2005) on the basis of available EIS photometry; M_U values have been calculated on the basis of observed V and $V-I$ to allow comparison with the CFRS values (see Sect. 4.3), and they might be affected by systematics at low redshift.

3. Description of the IMAGES catalog

Out of the 1142 slits placed, we could estimate redshifts for 691 objects, giving a success rate of ∼61%. Taking the 969 objects into account with $I_{AB} \leq 23.5$, we successfully estimated the redshift of 635 of them (success rate of 66%). The failure to estimate a redshift is associated mainly to low signal-to-noise (∼26%), objects falling near the edge of the slit (∼11%), and the presence of column of bad pixels (∼2%).

We observed 12 galaxies twice. By taking the difference between the two individual independent redshift measurements, we found a systematic uncertainty of 0.006 ± 0.014 in our redshift estimates. With the limited statistics available, we estimated a very conservative upper limit to the dispersion in our redshifts of 0.010.

In Fig. 3 we show the distribution of the redshifts for all galaxies and QSOs in our sample, consisting of all classes 2, 1, and 9. The mean and median of the distribution are 0.643 and 0.665, respectively. The strongest peaks in redshift are at 0.670 (82 objects, with $\Delta z = \pm 0.020$), at 0.735 (58), and at 0.210 (23). The first two peaks are in agreement with the existence of a "wall-like" structure in the CDFS (Le Fèvre et al. 2004; Gilli et al. 2003; Vanzella et al. 2005).

3.1. Completeness

The spectroscopic completeness, i.e. the ratio of the actual number of spectroscopic identifications obtained to that of total number of objects observed spectroscopically as a function of magnitude, helps in understanding the magnitude-dependent bias of the sample. As mentioned previously, for objects with $I_{AB} \leq 23.5$, the overall spectroscopic completeness is 66%. If we exclude the failures that have an instrumental origin, then the spectroscopic completeness for $I_{AB} \leq 23.5$ objects is 76%. In Fig. 4, we show the spectroscopic completeness achieved in measuring redshifts as a function of the apparent magnitude (I_{AB}).

In the upper panel the histogram of observed targets with $I_{AB} \leq 23.5$ is shown in white, while the black, green, and

[4] Table 2, where we provide the catalog is only available at the CDS.

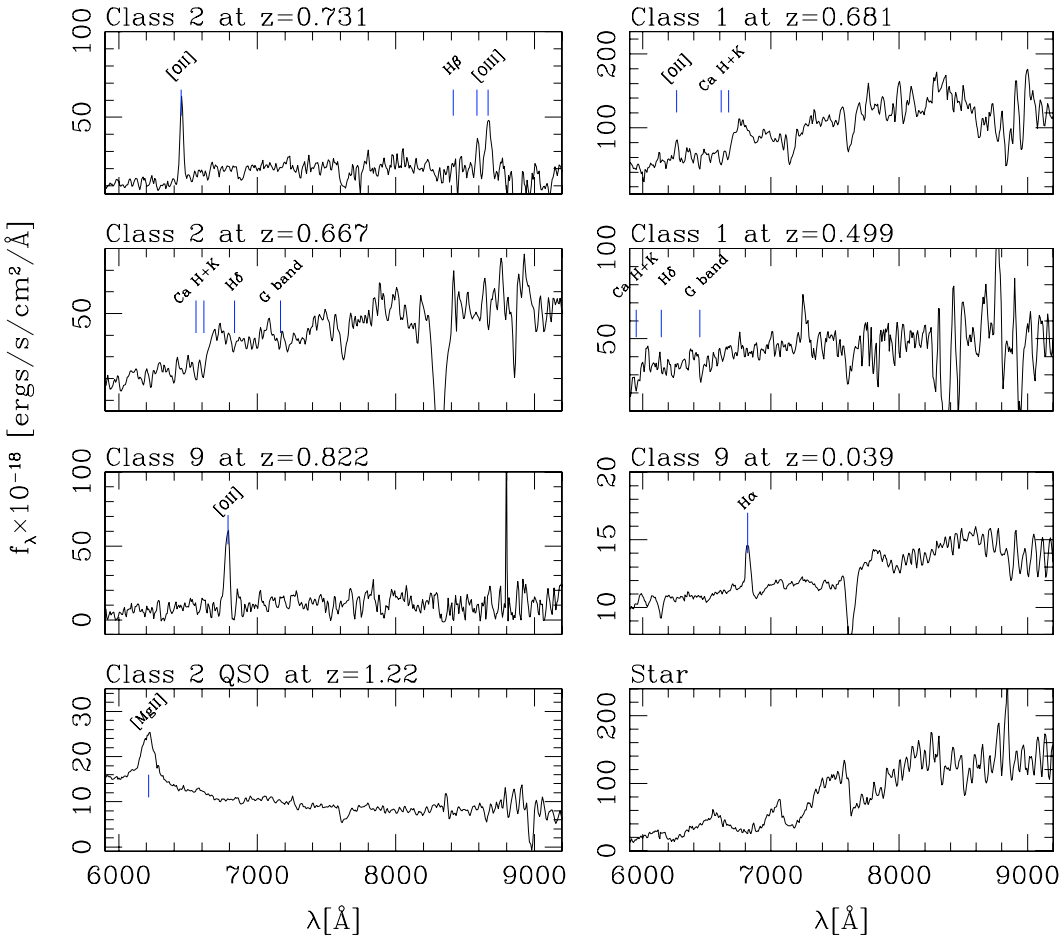

Fig. 2. Classification of spectra based on their quality. Sample spectra of various types and quality (class 2: secure, class 1: insecure, class 9: single line). *From top to bottom*: emission-line galaxies, absorption-line galaxies, single emission-line galaxies. *Bottom*: AGN and star.

blue histograms show the magnitude distribution of objects with redshift classes 2, 1, and 9, respectively. Further more, in Table 3, we compare the number of galaxy redshifts determined by IMAGES with the K20, VVDS, FORS2, and Szokoly et al. (2004). Our study represents about 35% of the galaxy redshifts available for objects with $I_{AB} \leq 22.5$ in the CDFS. The last column shows the number of galaxies observed in common from one survey to the others, based on the cross correlation of targets in the CDFS. 136 galaxies and 24 stars in IMAGES are found in common with other surveys, leaving us with 587 − 136 = 451 unique identifications of galaxy redshifts and 691 − 160 = 531 unique objects in IMAGES. For this comparison we have taken only reliable redshifts into account, with a confidence of at least 50%. This means that we used redshift estimations with flags 1, 2 and 9 from IMAGES, flags 1–4 and 9 from VVDS, flags 0 and 1 from K20, and all from FORS2[5]. The high efficiency, coupled with the relatively high completeness attained over a short exposure time highlights the advantage of low-resolution spectroscopy by VIMOS in estimating redshifts up to $z = 1.5$.

3.2. Comparison with other redshift estimations in the CDFS

We compared our redshift estimations with those publicly available in the CDFS, i.e. the VVDS (Le Fèvre et al. 2004), K20 (Cimatti et al. 2002), FORS2 (Vanzella et al. 2005; 2006), and the X-ray selected sample of Szokoly et al. (2004). We observed 98 objects in common with the VVDS, 42 with K20, 22 with FORS2, and 18 with Szokoly et al. samples. Because earlier surveys also included target duplications, we find that 160 IMAGES objects were already observed in them. For 76% of the common elements with VVDS, we have $\frac{\Delta z}{(1+z)} \leq 0.01$. The distribution of redshift difference for 56 objects where both VVDS and IMAGES mark a secured estimation shows $\sigma_{\Delta z} = 0.069$. We obtained similar percentages and dispersions for other samples too. In Fig. 5 we show the comparison of our redshift estimation with VVDS (shown as circles, open and filled), K20 (pentagons), FORS2 (squares) and Szokoly et al. (triangle) samples. The shaded and open symbols in Fig. 5 represent secure and insecure estimations, respectively. Clearly, all the significant differences arise from the low quality of the spectra in at least one of the surveys. Two of us (CDR & HF) compared the spectra of objects for which we obtained significantly different redshifts from VVDS, using the CENCOS database[6]. After comparison, we kept our redshift for about 60% of them. When spectral features did not match the VVDS ones (all with

[5] Note that the flags used by Vanzella et al. are not exactly similar to those used by other surveys, and flags 0.5, 1, 2, and 3 from Szokoly et al. were selected from Table 3. Excluding redshifts of objects already identified by other surveys (repeated observations, see Table 3), the IMAGES catalog produces 531 new redshift identifications, consisting of 307, 170, and 54 objects with class codes 2, 1, and 9, respectively. The catalog consists of 447 galaxies, 80 stars, and four quasars.

[6] http://cencosw.oamp.fr/FR/index.fr.html

Table 3. Comparison of the number (N) of galaxies (and AGN) with redshifts available in CDFS as a function of I_{AB} limiting magnitudes.

Sample	Time[a]	$I_{AB} \leq 22.5$	$I_{AB} \leq 23.5$	$I_{AB} \leq 24$	All	Common
K20	–	169	236	256	459	133
VVDS	265	552	1089	1460	1460	223
FORS2	281	127	219	308	711	144
Szokoly	114	77	89	90	121	55
IMAGES	45	376	532	569	587	136
Unique Identifications						
ALL	–	1068	1846	2328	2781	–
IMAGES	–	280	401	435	451	–
%[b]	–	35.5	27.8	23.0	19.4	–

[a] Approximate average exposure time per slit in minutes. The higher integration times used by other studies were justified by their scientific goals.
[b] The percentage of galaxies with new redshift identifications from the IMAGES survey. Calculated as IMAGES/(ALL – IMAGES).

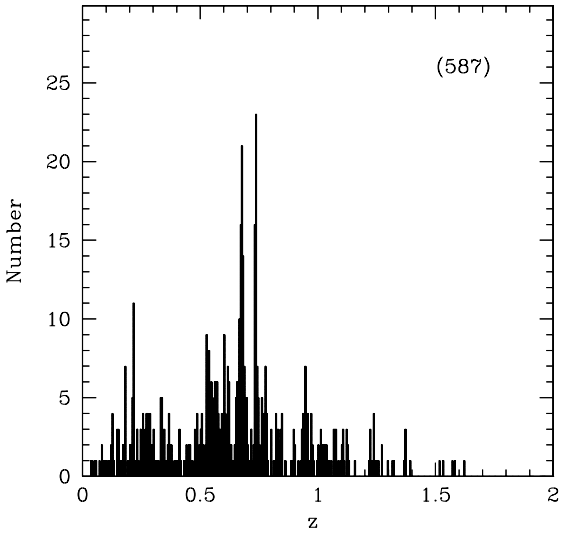

Fig. 3. Histogram of redshifts for galaxies and QSOs in our sample, comprising the classes 2,1, and 9. The size of the redshift bin is 0.005. The distribution shows prominent peaks at 0.210, 0.530, 0.670, and 0.735.

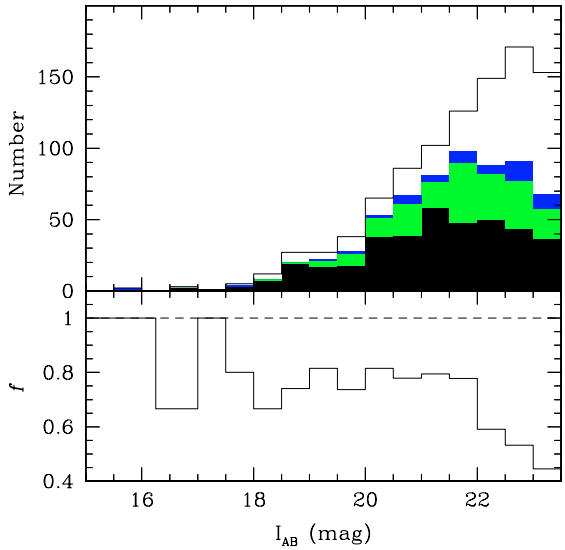

Fig. 4. Redshift measurement completeness for the $I_{AB} \leq 23.5$ sample in IMAGES. In the upper panel, we show the magnitude distribution of objects with a redshift class 2 (black), 1 (green), and 9 (blue), along with that for the observed targets (open). The lower panel shows the histogram of the fraction (f) of objects with redshifts compared to the total observed from IMAGES. We measure redshifts for 66% of the target objects, while the completeness achieved is 76% when we exclude failures that have an explicit instrumental origin.

very poor quality), we preferred our estimates because it appeared likely that the features in the VVDS spectra are artificial and arise from a failure by their automated data reduction to handle accurate sky subtraction and/or wavelength calibration. This was always possible anyway, since the VVDS team itself assigned the sources that we found to have discrepant redshifts of very poor quality. The redshift estimation for the object EISJ033235.64-274633.0 is noteworthy. We estimate a redshift of 0.564, while the VVDS team reports 3.6664 (GOODS identification J033235.62-274632.8) with their quality flag 2. We find the [OII]λ3727 emission at 5837.9 Å, although with a class = 1 as no more strong features were observed. The B band detection of the object ($B = 24.11$) also suggests the absence of the Lyman break feature corresponding to $z = 3.6664$, thus supporting our estimation of the lower redshift. This just highlights that caution should be observed when using redshift estimates of marginal or poor quality.

3.3. Stars and galaxies in the color–color diagram

The color–color diagram provides an easy tool for identifying possible mis-classifications of stars and galaxies. However, there may be an overlap between the colors of stars and galaxies, especially for the bluest objects (e.g., Crampton et al. 1995). In Fig. 6, the variation of $B - I$ as a function of $I - K$ is shown. Stars and galaxies with secure spectroscopic identifications are shown as filled triangles and squares, respectively, while the respective open symbols represent less secure ones. Using the diagram, we selected objects for visual examination, wherever possible, through the available HST-ACS and the GEMS images. We noticed 26 (4% of total objects with spectroscopic redshift) obvious cases of galaxies identified as stars (insecure, with class 1) in the preliminary catalog. Due to this uncertainty induced by inspecting the images, the quality flag of these objects were degraded to unidentified (class 0) in the final catalog.

3.4. Magnitude distribution

The variation of the apparent I magnitude as a function of redshift for the galaxies in our IMAGES catalog is shown in Fig. 7 differentiating secure and less secure redshift identification. We have estimated the absolute magnitudes following the method outlined in Hammer et al. (2001, 2005). The distribution of absolute magnitude (M_B) versus redshift is shown in Fig. 8, indicating the absolute magnitude depth attained by our observations.

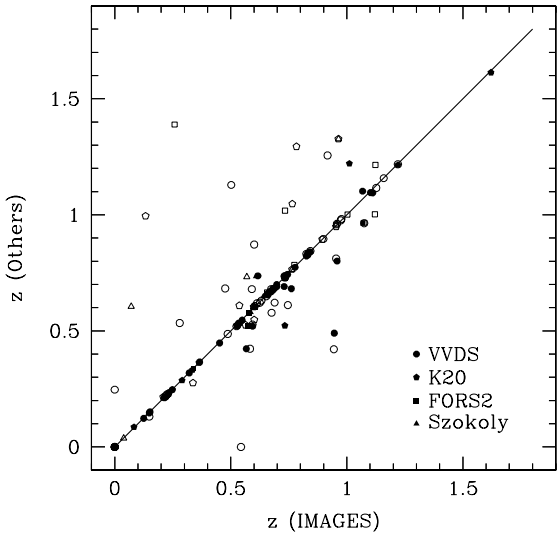

Fig. 5. The comparison of our redshift estimation with VVDS (open and shaded circles), K20 (open and shaded pentagons), FORS2 (open and shaded squares), and Szokoly (open and shaded triangles). The open symbols identify objects for which at least one of the surveys considers the redshift as insecure (for example, with flags 1 and 9 in both IMAGES and VVDS), otherwise a full symbol is adopted.

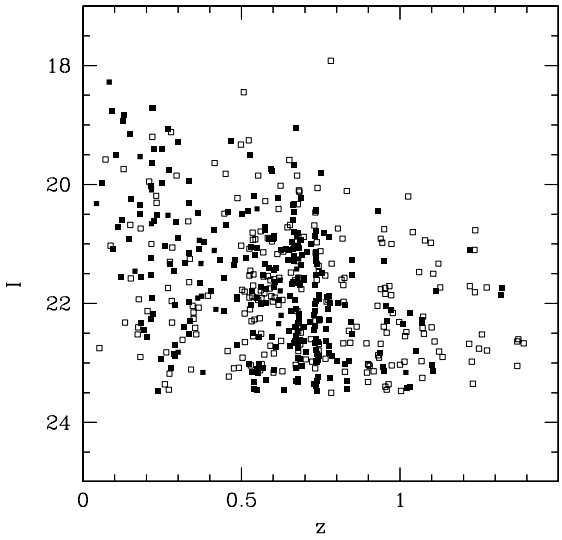

Fig. 7. The variation in the apparent I magnitude as a function of redshift for galaxies for which redshifts are measured by the IMAGES survey. Filled and open squares show secure and insecure redshift estimates, respectively.

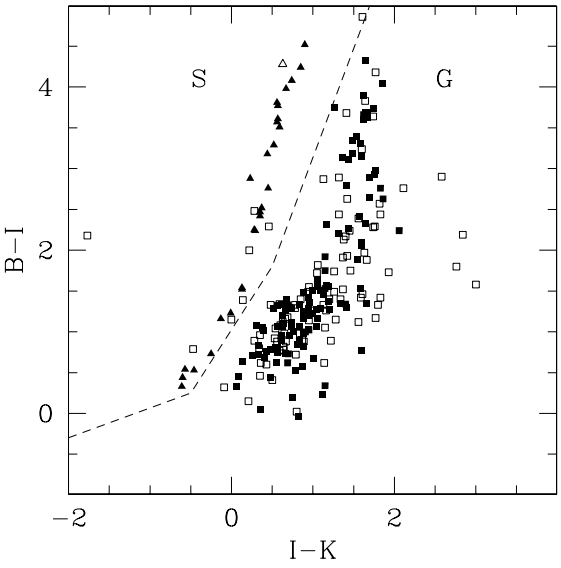

Fig. 6. The $I - K$ vs. $B - I$ diagram for stars (triangles) and galaxies (squares) with spectroscopic redshift measurements from IMAGES. Filled and open symbols represent secure and insecure redshift estimates, respectively. The dashed line roughly delineates the regions occupied by stars (S) and galaxies (G).

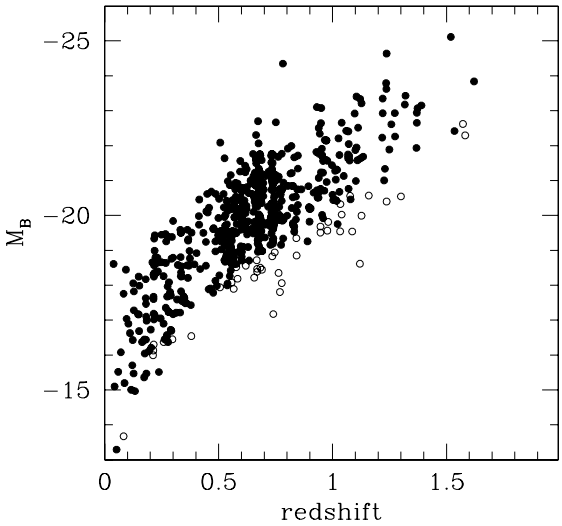

Fig. 8. Redshift vs. absolute M_B magnitude for objects in our sample showing the depth attained by our observation. Objects brighter and fainter than $I_{AB} = 23.5$ are shown as filled and open circles, respectively.

3.5. The sample of emission line galaxies in the IMAGES survey

One of the main criteria for selecting our sample of intermediate mass galaxies is the absolute magnitude selection $M_J \leq -20.3$. Such a limit corresponds to a stellar mass of $1.5 \times 10^{10} M_\odot$ when converting the J band luminosity using the prescription discussed in Bell et al. (2003; see also Hammer et al. 2005). However, the near- infrared observations in J, H, and K, essential for estimating M_J using the method of Hammer et al. (2005), are currently available only for the GOODS area, which forms a subset of the larger CDFS. But we find for galaxies in our sample with both B and J magnitudes that about 95% of $M_B \leq -20.0$ galaxies have $M_J \leq -20.3$. We obtained a very similar percentage with a much larger sample of galaxies with photometric redshift (from COMBO-17, see Wolf et al. 2004). This test was conducted in order to verify that the selection biases involved in our sample (also see Sect. 4.1) do not affect the fraction of $M_J \leq -20.3$ galaxies that could have $M_B > -20$. Hence for emission-line galaxies falling outside the area covered by the GOODS, we select our sample using the $M_B \leq -20.0$ criterion. In Fig. 9, we show the histograms of emission line galaxies available in CDFS. The IMAGES survey identifies 69 galaxies with $M_J \leq -20.3$ and [OII]λ3727 emission lines observable through GIRAFFE, while 68 are available from the VVDS survey. We also identify 157 emission-line galaxies with $M_B \leq -20.0$ for further observation, thus providing a large enough sample of target galaxies for detailed analysis, as envisaged in the IMAGES program.

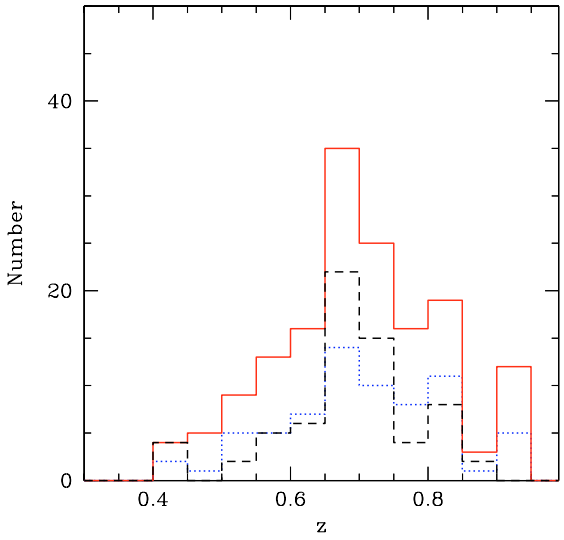

Fig. 9. Sample of galaxies that are candidates for GIRAFFE follow-up observations. The blue dotted histogram shows [OII]λ3727 emission galaxies with $M_J \leq -20.3$, identified from the IMAGES survey, while the black dashed histogram shows the one from the VVDS. The histogram with a continuous red line shows the distribution of emission line galaxies with $M_B \leq -20.0$, but with no M_J data available. See text for more details.

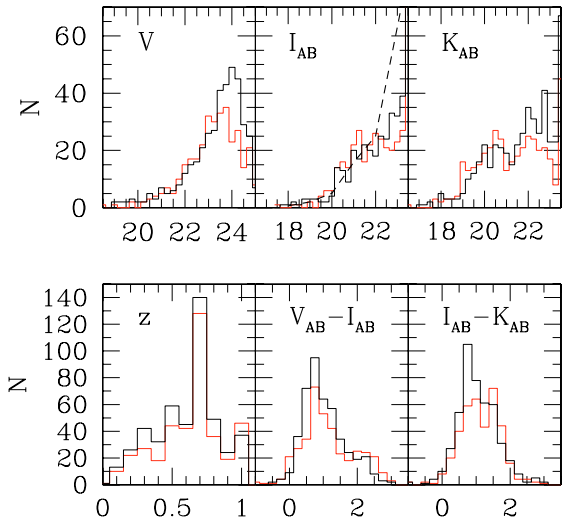

Fig. 10. Comparison between the distribution of VVDS (black histogram) and IMAGES+FORS2 (red histogram) galaxies in the GOODS field. From left to right, top to bottom, the two distributions are compared in V, I_{AB}, K_{AB}, z, $(V-I)_{AB}$, and $(I-K)_{AB}$, respectively. Kolmogorov-Smirnov tests show that the associated probabilities (for the two samples to be derived from the same population) are 96, 99.999, 82, 78, 96, and 99.999%, respectively. Notice that a Pearson test provides similar numbers (probabilities always higher than 91%). The dashed line in the top-middle panel represents the counts in the I band (see Arnouts et al. 2001), showing that both catalogs are missing galaxies at the faint end.

In what follows, we provide a representative sample of galaxies with spectroscopic redshift in the GOODS field to address the issues related to the possible cosmological variance within this field.

4. The representativeness of GOODS-South for cosmological studies

The GOODS project envisages the use of the best and probably the deepest multi-wavelength data in order to understand various cosmological problems like the formation and evolution of galaxies and active galactic nuclei, and the distribution of dark matter and the large scale structure at high redshifts. However, after this region was chosen, it was discovered that it had a "wall-like structure" (Le Fèvre et al. 2004; Gilli et al. 2003; Vanzella et al. 2005). Finding such a correlation in the galaxy distribution necessitates a more detailed analysis of issues related to the cosmological variance that might affect our understanding of galaxy evolution when using data from the CDFS region.

To conduct this investigation, we constructed a sample of galaxies with reliable spectroscopic redshifts in the GOODS area by combining the IMAGES data with other relevant, publicly available spectroscopic redshift surveys. The sample is then used to compare the global properties of galaxies observed in the CFRS. The CFRS (see Crampton et al. 1995) is a collection of data on and analysis of galaxies with $I_{AB} < 22.5$, selected in an unbiased way from 5 distinctly uncorrelated areas of 100 arcmin^2 in the sky to mitigate the effects of cosmic variance (see Fig. 8 in Crampton et al. showing the redshift distribution of the 5 individual fields). Although significantly less deep than the observations in the GOODS, the CFRS provides an ideal sample to test the possible impact of cosmic variance in the GOODS region.

4.1. The GOODS – South field spectroscopic catalog: 640 galaxies with $I_{AB} \leq 23.5$ and $z \leq 1$

Although the IMAGES survey was highly efficient in estimating redshifts, the short integration time of the survey introduces a real bias towards brighter galaxies. This is evident in Fig. 4 as the fraction of redshift-identified objects becomes low at fainter magnitudes ($I > 22$). Moreover, the high efficiency of the IMAGES survey is mainly reflected in its ability to obtain redshifts for galaxies with strong emission-line spectra. The short integration time results in low signal-to-noise for faint objects, which in turn causes serious difficulties in estimating redshifts of galaxies showing absorption line only or weak emission lines. Thus we tend to be particularly biased against obtaining redshifts for the fainter early-type galaxies. On the other hand, we find that the selection criteria employed by the FORS2 team lead to spectroscopically identifying those objects that are largely missed by IMAGES. The FORS2 spectroscopic team generally selected redder and fainter galaxies, significantly helping to overcome the biases in our spectroscopic survey. The VVDS catalog forms a more complete sample (84% completeness for objects with $I_{AB} \leq 24$).

Here we limit our analysis to GOODS-South galaxies with $I_{AB} \leq 23.5$ and $z \leq 1$, with the aim of testing the cosmological relevance of the GOODS-South field within that redshift range. Figure 10 compares the properties of galaxies in VVDS (337 galaxies) to those of the combined sample of IMAGES and FORS2 (303 galaxies). It reveals a remarkable consistency between the two samples, whose photometric, color, and redshift distributions are almost indistinguishable on the basis of statistical tests. In the following we combine the two catalogs, assumed to provide a representative sample of $z \leq 1$ galaxies up to $I_{AB} = 23.5$. In the following, the GOODS – South field spectroscopic catalog corresponds to the combination of the VVDS and of IMAGES and FORS2 catalogs in the GOODS field.

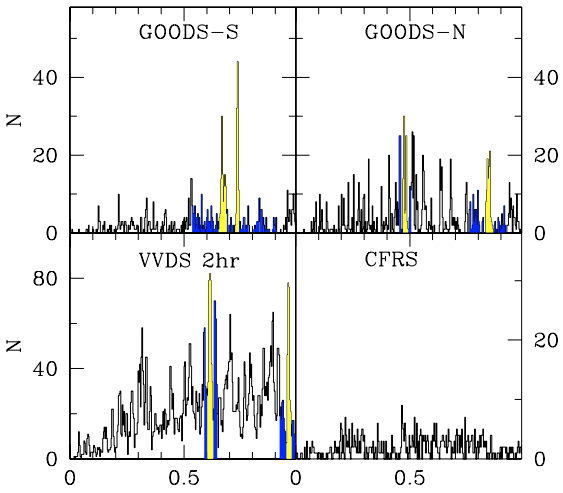

Fig. 11. Comparison between the redshift distribution of GOODS-S ($I_{AB} \leq 23.5$, this paper) redshift ditribution to that of GOODS-N ($R_{AB} \leq 24.5$, Wirth et al. 2004), VVDS02h ($I_{AB} \leq 24$, Le Fèvre et al. 2005), and CFRS ($I_{AB} \leq 22.5$, Crampton et al. 2005). In yellow are shown the two most prominent structures in GOODS-S, GOODS-N, and VVDS02h. In blue are identified the redshift area surrounding the structure, which contains the same number of galaxies as the two largest structures.

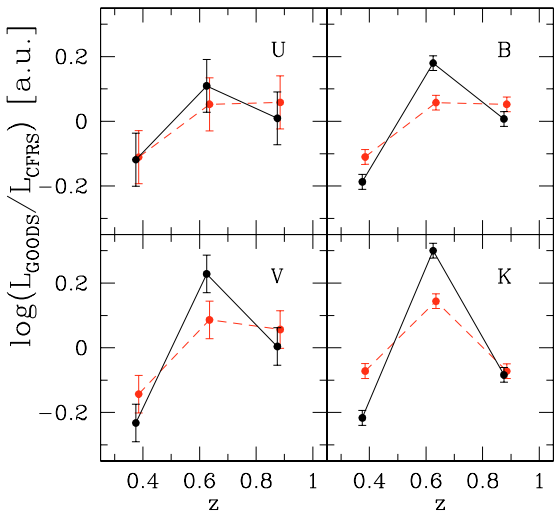

Fig. 12. Evolution in the ratios of luminosity densities of observed galaxies from the GOODS spectroscopic sample and observed galaxies from CFRS as a function of redshift, for 3 redshift bins (0.25–0.5; 0.5–0.75, and 0.75–1). Black and red-dashed lines correspond to values calculated using the spectroscopic and photometric redshifts, respectively.

4.2. Comparison of the GOODS-S redshift distribution to that of GOODS-N, VVDS02h and CFRS

We retrieved from the literature existing redshift surveys of similar depths than our GOODS-S sample. Figure 11 presents the 4 redshift histograms, revealing in three cases (GOODS-S, GOODS-N, and VVDS02h) the existence of large-scale structures. As noticed above, the CFRS is a blend of 5 different fields of view, so the combination has smeared the large-scale structures. For each field we identified the two most prominent structures, and identify the redshift area surrounding the structure, which contains the same number of galaxies as the two structures. This is similar to an "equivalent (redshift) width" revealing the impact of the structure in a given redshift survey. The two prominent structures in GOODS-S, GOODS-N, and VVDS02hr provide equivalent (redshift) widths of $\Delta z = 0.317$, 0.148, and 0.09, respectively. It is unlikely that these differences can be related to the (small) differences in limiting magnitudes. Knowing that many studies of the evolution of integrated quantities, such as SFR or stellar mass densities, consider redshift bins of Δz from 0.25 to 0.5, this clearly requires more investigations to understand if GOODS-S field can be biased by the presence of such prominent large-scale structures. In the following, we test their impact in deriving luminosity density by comparing with the CFRS, which is by construction, not affected by structures.

4.3. Comparison of the luminosity evolution from GOODS-S with that from CFRS

The CFRS sample was selected solely by the $I_{AB} \leq 22.5$ criterion, and it includes 591 galaxies, among which 576 have $z \leq 1$. The GOODS spectroscopic catalog contains 428 $I_{AB} \leq 22.5$ galaxies, including 405 with $z \leq 1$. The number of objects with $I \leq 22.5$ forms about 49% of those present within this magnitude limit in the GOODS area, and Fig. 10 (see upper middle panel) shows that it is a fair representation of $I \leq 22.5$ galaxies. In Fig. 12 we show the redshift variation of the ratios of luminosity densities of observed galaxies from the GOODS catalog with those from the CFRS, for galaxies with $0.25 \leq z \leq 1$, using 3 redshift bins. Recall that luminosity densities are evaluated from integrating the luminosity functions, which are themselves estimated from the distribution of observed galaxies. Any difference between the distribution of observed galaxies in two distinct areas would undoubtedly generate a similar difference in the derived luminosity densities. Figure 12 proves that GOODS-South field displays a strong excess of luminosity densities in the $z = 0.5$–0.75 bin, at B, V, and especially at K wavelengths. We interpret this as related to a large-scale structure (i.e. cosmic variance) because more than half of the GOODS-South galaxies in that bin are found in two large-scale structures (see Fig. 11). Besides this, the shape of the U luminosity density evolution is far less affected, providing that the star formation rate density from UV light is almost comparable from GOODS-South to CFRS. Nevertheless, Fig. 12 suggests that one has to be cautious in interpreting evolution of the stellar mass density on the sole basis of the GOODS-South or the CDFS galaxies, since it is particularly related to the K luminosity density evolution. In the next section, we test more accurately why the large-scale structures in GOODS-South tend to affect red luminosity densities more than those at blue wavelengths.

To understand whether the cosmic variance related to the CDFS/GOODS-South field might affect analysis of galaxy evolution, we show in Fig. 12 the evolution of ratios of luminosity densities for galaxies upto $z = 1$, from the CFRS and the GOODS spectroscopic sample. Calculations of the absolute luminosities were done following Hammer et al. (2005). For consistency reason we derived the K_{AB} band luminosities in CFRS using $K_{AB} = K' + 1.87$ (as in GOODS), instead of $K_{AB} = K' + 1.78$ used in Lilly et al. (1995). There is no noticeable variation in the evolution of U luminosity density between the samples, while the B, V, and K light shows increasingly significant variations. We find the presence of large-scale structure in the GOODS responsible for this. Dashed (red) lines show a similar relation, but with adopting photometric redshifts from Wolf et al. (2004) instead of spectroscopic redshifts. Error bars correspond to Poisson statistics combined with photometric errors from measurements (see Arnouts et al. 2001) and from

calculations of the absolute magnitudes. Photometric errors at U, B, V, and K wavelengths are found to be 0.07, 0.02, 0.05, and 0.02 dex median values from Arnouts et al. (2001), respectively.

Interestingly, most of the signatures of the large-scale structures disappear in the intermediate bin, except a signal in the K band. An examination of the distribution of photometric redshifts (see Fig. 10 in Wolf et al.) indeed shows that the large-scale structures are somewhat recovered, but are much less prominent than in Fig. 11 (upper-left panel). For example, with photometric redshifts, the two prominent structures at $z = 0.670$ and $z = 0.735$ have merged, and the corresponding "equivalent width" is $\Delta z \sim 0.08$, to be compared to $\Delta z = 0.317$ when using spectroscopic redshifts. Thus, we wonder if some of the evolutionary trends found using photometric redshift surveys cannot be misunderstood as related to the CDFS large-scale structures.

4.4. Evolution of galaxies inside and outside the structures in the GOODS

It is understood that the environments in which galaxies reside have a significant influence on their formation and evolution. To analyze the properties of galaxies inside and outside the structures, we designated galaxies in the field and in the structures as shown in Fig. 13a. The redshift range for field galaxies were selected so that each sample contained similar numbers of galaxies while the structures were defined solely as regions with significant excesses. In the other subpanels of Fig. 13, we show the distribution of U, V, and K luminosities of galaxies inside and outside the redshift spikes. The two distributions in U are not significantly different, overall suggesting a similarity in their star-formation rates. However, for K, there is significant difference in the distributions as the galaxies in the structures are likely to be more massive on average, while there is a difference in the case of the comparison of the V-band luminosities, but it is statistically weaker. Testing each distribution with a Kolmogorov-Smirnov statistic confirms our visual impression, suggesting that the significance of the similarity in each pairs of histograms is 73, 2, and 0.6% for U, V, and K, respectively. This implies that the distribution of K-band magnitudes is significantly different, the V-band magnitude distributions are only marginally different, and the U-band magnitude distribution are statistically the same. It is particularly interesting to note that the (UV-traced) star formation rate does not differ significantly for galaxies inside the structures and the field. But the existence of what are likely to be more massive galaxies in the structures suggests that the specific star formation rate of galaxies in the structure lower than in the rest of the sample, implying that they are more evolved. This provides evidence that the evolution of galaxies in and around denser environments is faster than those in the field. In summary, the presence of large-scale structures in the CDFS/GOODS-South field might also affect studies of the specific star formation and its evolution.

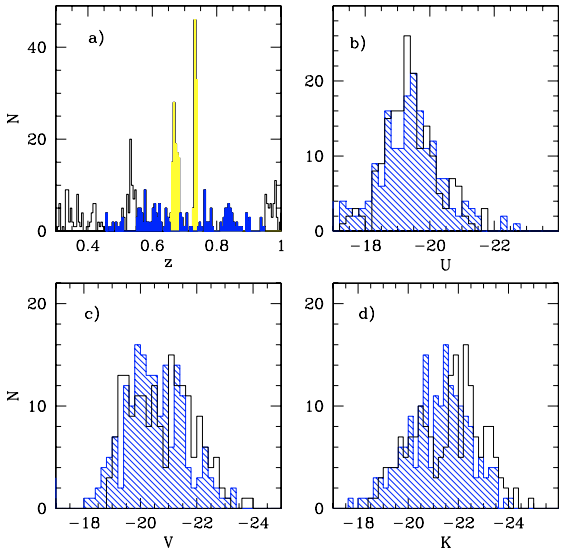

Fig. 13. Comparison of histograms of luminosities inside and outside the large-scale structures present in CDFS. In **a)**, the regions selected to represent the structure (yellow) and the field (blue) are shown. The redshift range for the galaxies in the two main structures is defined by 0.735 ± 0.009 and 0.668 ± 0.016, while the field galaxies are taken from 0.7 ± 0.25, excluding the structures mentioned above, and the smaller one at 0.530 ± 0.020. In **b)–d)** we show the distributions of U, V, K luminosities inside (open histogram) and outside (blue shaded) the structures.

5. Conclusion

This paper prepares a series analyzing the formation and evolution of intermediate massive galaxies at intermediate redshifts. Here we report the determination of new spectroscopic redshifts in the Chandra Deep Field South, using low-resolution VIMOS observations. We were able to spectroscopically identify 691 objects, consisting of 580 galaxies, 104 stars, and seven QSOs. Employing an integration time of 45 min for two pointings with VIMOS, this study increases by 28% (and 35%) the availability of $I_{AB} \leq 23.5$ (and $I_{AB} \leq 22.5$) galaxies with redshift, which were poorly represented in the existing redshift surveys. The redshift distribution contains major peaks at 0.670 and 0.735, supporting the existence of the large-scale structures already detected by the VVDS and FORS2 surveys. The presence of large-scale structures can raise various issues related to the cosmological variance of the GOODS. To analyze them, we constructed a representative catalog of 640 galaxies with spectroscopic redshift with $I \leq 23.5$ and $z \leq 1$. Hence we attempted to analyze the "cosmological representativeness" of the GOODS region by studying the properties of galaxies in GOODS in comparison with those of other surveys, including the CFRS. It turns out that the GOODS-South field is by far the most affected by the presence of large-scale structures.

We do find a strong excess of luminosity density at $z = 0.5$–0.75 in GOODS-South when compared to CFRS, especially in the V and K bands. This suggests that studies related to the evolution of the stellar mass and/or of the specific star formation rate need to be interpreted cautiously. By analyzing the galaxies inside and outside the structures in the GOODS field we find that the galaxies in the structure tend to be more massive and evolved compared to those outside the structures. This is very likely at the origin of the excess luminosity density found at this redshift in the GOODS-South. Such an effect is found to be less prominent by using photometric redshifts instead of spectroscopic redshifts. However, on the sole basis of photometric redshifts in that field, it does not seem easy to disentangle effects related to galaxy evolution from those arising from the presence of large-scale structures, because structures appear less prominent due to the uncertainties of the redshift determination. Spectroscopic redshifts are then very essential for galaxy evolution studies.

The GOODS South field has been observed with an unprecedented depth at many wavelengths including optical and IR. It is one of the most studied cosmological fields, which has generated a large number of papers about the galaxy evolution. We stress

that many of these studies could be affected by cosmological variance of this field as revealed by our relatively modest spectroscopic study. We believe that this might affect some conclusions in studies based on photometric redshifts, especially those related to the evolution of stellar mass density and of specific star formation rate. Studies based on spectroscopic redshifts, such as IMAGES, also have to carefully compare the evolutionary properties of galaxies inside and outside the structures, before concluding about an overall picture of galaxy evolution.

Acknowledgements. We thank the Centre Franco-Indien pour la Promotion de la Recherche Avancee (CEFIPRA) for a post-doctoral fellowship (CDR) and financial assistance (AR and FH). We warmly thank our referee for his/her detailed comments and suggestions, which have contributed a lot toward improving our manuscript.

References

Appenzeller, I., Fricke, K., Furtig, W., et al. 1998, The Messenger, 94, 1
Arnouts, S., Vandame, B., Benoist, C., et al. 2001, A&A, 379, 740
Bell, E. F. McIntoch, D. H., Katz, N., et al. 2003, ApJS, 149, 289
Cimatti, A., Mignoli, M., Daddi, E., et al. 2002, A&A, 392, 395
Crampton, D., Lilly, S., Le Fèvre, O., Hammer, F. 1995, ApJ, 455, 96
Elbaz, D., Cesarsky, C. J., Chanial, P., et al. 2002, A&A, 384, 848
Flores, H., Hammer, F., Thuan, T., et al. 1999, ApJ, 517, 148
Flores, H., Puech, M., Hammer, F., Garrido, O., & Hernandez, O. 2004, A&A, 420, 31
Flores, H., Hammer, F., Puech, M., Amram, P., & Balkowski, C. 2006, A&A, 455, 107
Gilli, R., Cimatti, A., Daddi, E., et al. 2003, ApJ, 592, 721
Hammer, F., Gruel, N., Thuan, T. X., Flores, H., & Infante, L. 2001, A&A, 550, 570
Hammer, F., Flores, H., Elbaz, D., et al. 2005, A&A, 430, 115
Heavens, A., Panter, B., Jimenez, R., & Dunlop, J. 2004, Nature, 428, 625
Le Fèvre, O., Vettolani, G., Paltani, S., et al. 2004, A&A, 428, 1043
Le Fèvre, O., Vettolani, G., Garilli, B., et al. 2005, A&A, 439, 845
Le Floc'h, E., Papovich, C., Dole, H., et al. 2005, ApJ, 632, 169
Mignoli, M., Cimatti, A., Zamorini, G., et al. 2005, A&A, 437, 883
Navarro, J. F., Frenk, C. S., & White, S. D. M. 1997, ApJ, 490, 493
Puech, M., Hammer, F., Flores, H., Ostlin, G., & Marquart, T. 2006a, A&A, 455, 119
Puech, M., Flores, H., Hammer, F., & Lehnert, M. D. 2006b, A&A, 455, 131
Szokoly, G. P., Bergeron, J., Hasinger, G., et al. 2004, ApJS, 155, 271
Tully, R. B., & Fisher, J. R. 1977, A&A, 54, 651
Vanzella, E., Cristiani, S., Dickinson, M., et al. 2005, A&A, 434, 53
Vanzella, E., Cristiani, S., Dickinson, M., et al. 2006, A&A, 454, 423
Wirth, G. D., Willmer, C., Amico, P., 2004, AJ, 127, 3121
Wolf, C., Meisenheimer, K., Kleinheinrich, M., et al. 2004, A&A, 421, 913
Zheng, X. Z., Hammer, F., Flores, H., Assémat, F., & Pelat, D. 2004, A&A, 421, 847